Journal of Power Sources 224 (2013) 230–235

Contents lists available at SciVerse ScienceDirect

Journal of Power Sources

journal homepage: www.elsevier.com/locate/jpowsour

Thermal expansion in lithium manganese oxide spinels $Li[Li_xMn_{2-x}]O_4$ with $0 \leq x \leq 1/3$

Kazuhiko Mukai*, Yoshihiro Kishida, Hiroshi Nozaki, Kazuhiko Dohmae

Toyota Central Research and Development Laboratories, Inc., 41-1 Yokomichi, Nagakute, Aichi 480-1192, Japan

HIGHLIGHTS

- The coefficients of thermal expansion in $Li[Li_xMn_{2-x}]O_4$ with $0 \leq x \leq 1/3$ are examined.
- The coefficients of thermal expansion in $x = 0$ are very different between the orthorhombic axes.
- The coefficients of thermal expansion are almost independent on x at $x \geq 0.05$.

ARTICLE INFO

Article history:
Received 9 June 2012
Received in revised form
18 September 2012
Accepted 21 September 2012
Available online 10 October 2012

Keywords:
Lithium-ion battery
Coefficient of thermal expansion
Lithium manganese oxide
Spinel
Jahn–Teller transition

ABSTRACT

In order to know the coefficients of thermal expansion in lithium manganese oxide spinels $Li[Li_xMn_{2-x}]O_4$ with $0 \leq x \leq 1/3$, X-ray diffraction measurements are performed in the temperature (T) range from 400 to 100 K. The crystal structure for $x = 0$ changes from the high-T cubic phase ($Fd\bar{3}m$) into the low-T orthorhombic phase ($Fddd$) below 285 K due to a cooperative the Jahn–Teller transition. Hence, the average coefficients of linear thermal expansion (α_L) in $x = 0$ are very different between the three orthorhombic axes; $\alpha_L = 1.3(1) \times 10^{-6}\ K^{-1}$ along the a_o-axis, $\alpha_L = 13.1(1) \times 10^{-6}\ K^{-1}$ along the b_o-axis, and $\alpha_L = 5.7(1) \times 10^{-6}\ K^{-1}$ along the c_o-axis, where a_o, b_o, and c_o are the lattice parameters of orthorhombic phase. On the other hand, the crystal structure for the samples with $x \geq 0.05$ keeps the cubic phase ($Fd\bar{3}m$) down to 100 K. The α_L value is almost independent on x at $x \geq 0.05$, i.e. $\alpha_L \sim 7.0 \times 10^{-6}\ K^{-1}$. This suggests that the bond strength between Mn(Li) and O^{2-} ions does not increase by the partial substitution of Li ions for Mn ions.

1. Introduction

Due to increasing demand for secondary batteries with high energy density and long cycle-life, lithium-ion battery (LIB) has been heavily investigated over the past decade [1]. Although a liquid electrolyte consisted of lithium salt and organic solvents is used in the current commercial LIB, all solid-state LIB having a solid electrolyte is considered to be a next-generation battery. This is because one can increase the energy density of LIB by applying three-dimensional battery architectures [2]. Moreover, the side reactions leading to capacity fading are suppressed compared to the conventional LIB [3].

One of the biggest issues in realizing all solid-state LIB is how to construct the solid–solid interfaces. Lithium insertion materials such as $LiCoO_2$ [4–7], $LiNiO_2$ [8,9], etc. maintain these framework structures during the charge and discharge reactions. The extraction/insertion of lithium ions, however, induces the change in lattice parameters, namely, the change in lattice volume (ΔV), except for so-called zero-strain insertion material $Li[Li_{1/3}Ti_{5/3}]O_4$ [10]. Considering the application in the wide temperature (T) range above 100 K, not only the ΔV value, but also the coefficient of thermal expansion (CTE) in lithium insertion material is crucial information for constructing the solid–solid interfaces. Here, the thermal expansion in materials is explained by introducing the anharmonicity of lattice vibration to the interatomic potential energy [11,12]. Thus, the CTE would also provide an indicator of bond strength between atoms of lithium insertion materials as in the case for a large number of glasses, metals, and oxides [13]. Indeed, our recent X-ray diffraction (XRD) studies on Li_yCoO_2 indicate the anisotropic thermal expansion between the interplane and intraplane of the CoO_2 layer, suggesting a rigid network of edge-sharing CoO_6 octahedra. [7].

Lithium manganese oxide $Li[Li_xMn_{2-x}]O_4$ (LMO) with $0 \leq x \leq 1/3$ adopts the cubic spinel structure with $Fd\bar{3}m$ space group at room T [14–16], and consequently, shows smaller ΔV value than $LiCoO_2$ [5–7] and $LiNiO_2$ [9]. LMO is, hence, thought to be a suitable

* Corresponding author. Tel.: +81 561 71 7698; fax: +81 561 63 6156.
E-mail address: e1089@mosk.tytlabs.co.jp (K. Mukai).

0378-7753/$ – see front matter © 2012 Elsevier B.V. All rights reserved.
http://dx.doi.org/10.1016/j.jpowsour.2012.09.107

electrode material for all solid-state LIB. According to the previous structural analyses on LMO, LMO with $x = 0$ exhibits a structural phase transition from high-T cubic ($Fd\bar{3}m$) phase to low-T tetragonal ($I4_1amd$) [17,18] phase or orthorhombic ($Fddd$) [19–21] phase at around 285 K. Furthermore, LMO with $x = 1/3$ contains small amount of Li_2MnO_3 impurity [22–24]. On the electrochemical tests, LMO with $x = 0$ shows poor cycle performance even at room T [16,25,26], while LMO with $x \geq 0.05$ shows relatively stable cycle life at room T [25–28]. Despite of the extensive studies on LMO, the coefficients of linear thermal expansion (α_L) and volumetric thermal expansion (β_V) of LMO are still unknown. We have, therefore, performed a systematic XRD study on LMO in the T range 400 to 100 K, in order to know both T dependence of lattice parameters and x dependence of CTE. In this paper, we report the α_L and β_V for LMO together with those for other lithium insertion materials.

2. Experimental

Powder samples of LMO with $x = 0$, 0.05, 0.1, 0.15, 0.2, and 1/3 were prepared by a two-step solid-state reaction technique [24,27] in order to obtain highly crystallized LMO samples. The reaction mixture of $LiOH \cdot H_2O$ and MnO_2 was well mixed with a mortar and pestle, and pressed into a pellet of 23 mm diameter and ~5 mm thickness. The pellet was heated at 1273 K in air for 12 h, then the obtained powder was crushed and repressed into a pellet again, and finally the pellet was oxidized at 1073 K for 24 h, 923 K for 24 h, 873 K for 24 h, 823 K for 48 h, and 773 K for 48 h in air without cooling down to room T.

The electrochemical reactivity for LMO was examined in a nonaqueous lithium cell. In preparing the electrode, polyvinylidene fluoride (PVdF) dissolved in N-methyl-2-pyrrolidone solution was used as a binder. The black viscous slurry consisting of 88 wt% LMO powder, 6 wt% acetylene black, and 6 wt% PVdF was cast on an aluminum foil with blade. The electrode (ϕ 16 mm) was dried under vacuum at 393 K for 12 h. The lithium metal sheet pressed on a stainless steel plate (ϕ 19 mm) was used as a counter electrode. Two sheets of porous polyethylene membrane (Tonen-General Sekiyu K. K., Japan) were used as a separator. The electrolyte was 1 M $LiPF_6$ dissolved in ethylene carbonate (EC)/dimethyl carbonate (DEC) (1/1 volume ratio) solution (Kishida Chemical Co. Ltd., Japan).

XRD measurements were carried out in the T range from 400 to 100 K at a synchrotron radiation facility of SPring-8 (BL19B2). For the $x = 0$ sample, XRD measurements were also made in the T range from 287.5 to 275 K. After reaching the every setting T, we took the waiting time for 3 min to stabilize the T of the sample. The T of the sample during the XRD measurements was controlled by a continuous N_2-flow device (CGD-1, Rigaku Co. Ltd., Japan) with a precision of ±0.1 K. The wavelength of the X-ray was estimated as 0.70000(1) Å by the XRD measurements on NIST CeO_2 standard (674a). All the LMO samples were packed into a boro-silicate glass capillary tube with 0.3 mm diameter. The Rietveld analyses were performed by RIETAN2000 [29].

3. Results

3.1. XRD patterns of $Li[Li_xMn_{2-x}]O_4$

Fig. 1 shows the XRD patterns of the LMO samples with (a) $x = 0$, (b) $x = 0.1$, (c) $x = 0.2$, and (d) $x = 1/3$ at 400 K. The XRD patterns for the $x = 0$, 0.1, and 0.2 samples are identified as a single phase of the spinel structure with space group of $Fd\bar{3}m$, in which Li^+ ions occupy both the tetrahedral 8a and octahedral 16d sites and Mn ions sit the octahedral 16d site. On the contrary, for the $x = 1/3$ sample, the

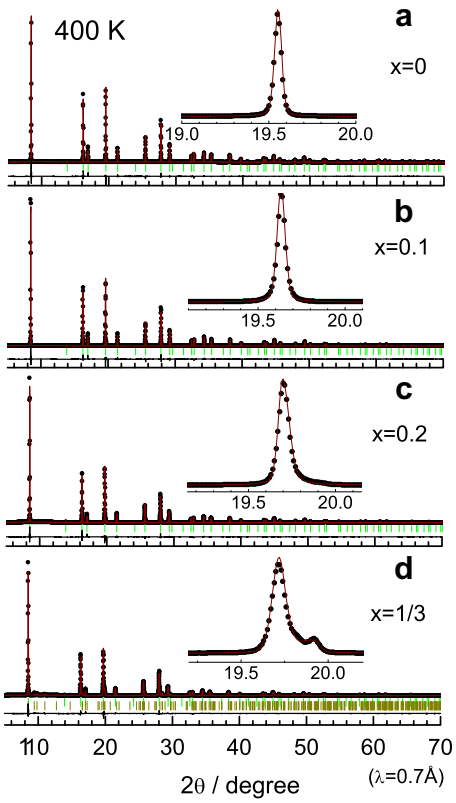

Fig. 1. XRD patterns of the $Li[Li_xMn_{2-x}]O_4$ samples with (a) $x = 0$, (b) $x = 0.1$, (c) $x = 0.2$, and (d) $x = 1/3$ at 400 K. The enlarged diffraction line (major diffraction line) in the inset corresponds to the 400 diffraction line of the cubic spinel structure.

weak diffraction lines are observed in the higher diffraction angle in the vicinity of the major diffraction lines. This is clearly understood by the enlarged diffraction line around $2\Theta = 20^\circ$ (see the inset in Fig. 1 (d)). According to the previous studies on $Li[Li_{1/3}Mn_{5/3}]O_4$ [22–24], the Li_2MnO_3 impurity with a monoclinic ($C2/m$) structure inevitably coexists in the sample due to the extremely slow reaction rate of $(1-x)LiMn_2O_4 + xLi_2MnO_3 + x/2O_2 \rightarrow Li[Li_xMn_{2-x}]O_4$. The XRD pattern for the $x = 1/3$ sample is, thus, assigned as a mixture of the spinel phase ($Fd\bar{3}m$) and the Li_2MnO_3 phase ($C2/m$). The weight fraction of the Li_2MnO_3 phase [$W(Li_2MnO_3)$] in the $x = 1/3$ sample is estimated to be ~0.11 by following equation:

$$W_p = S_p(ZMV)_p \Big/ \sum_{i=1}^{n} S_i(ZMV)_i, \quad (1)$$

where W is the relative weight fraction of the phase p in a mixture of the n phase, S the Rietveld scale factor, Z the number of formula units per unit cell, M the mass of the formula unit, and V the unit cell volume, respectively. The XRD patterns at 300 K (not shown) are essentially the same to those at 400 K; the XRD patterns for $x \leq 0.2$ are assigned as the single spinel phase ($Fd\bar{3}m$), while the XRD pattern for $x = 1/3$ is assigned as the mixture of the spinel phase ($Fd\bar{3}m$) and the Li_2MnO_3 phase ($C2/m$).

Fig. 2 shows the XRD patterns of the $Li[Li_xMn_{2-x}]O_4$ samples with (a) $x = 0$, (b) $x = 0.1$, (c) $x = 0.2$, and (d) $x = 1/3$ at 100 K. As clearly seen in the inset of Fig. 2(a), three diffraction lines are observed around $2\Theta = 20^\circ$, suggesting a structural phase transition below 300 K. Although the crystal structure of stoichiometric $LiMn_2O_4$ below room T is different among the research groups [17–21], there seems to be general agreements that the onset of the structural phase

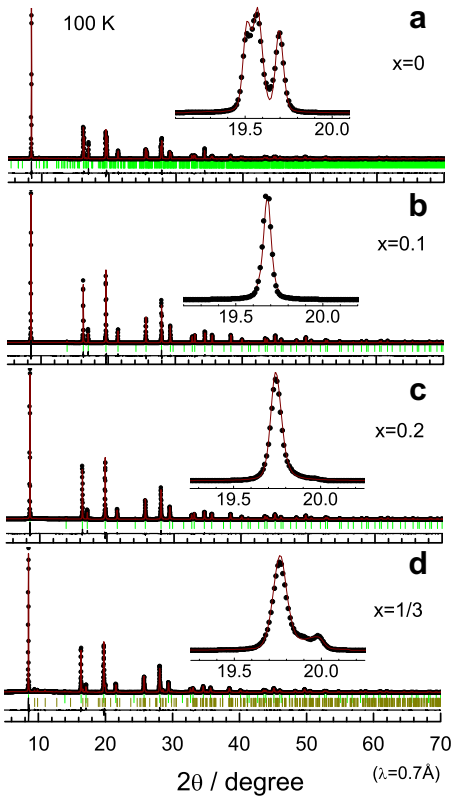

Fig. 2. XRD patterns of the $Li[Li_xMn_{2-x}]O_4$ samples with (a) $x = 0$, (b) $x = 0.1$, (c) $x = 0.2$, and (d) $x = 1/3$ at 100 K.

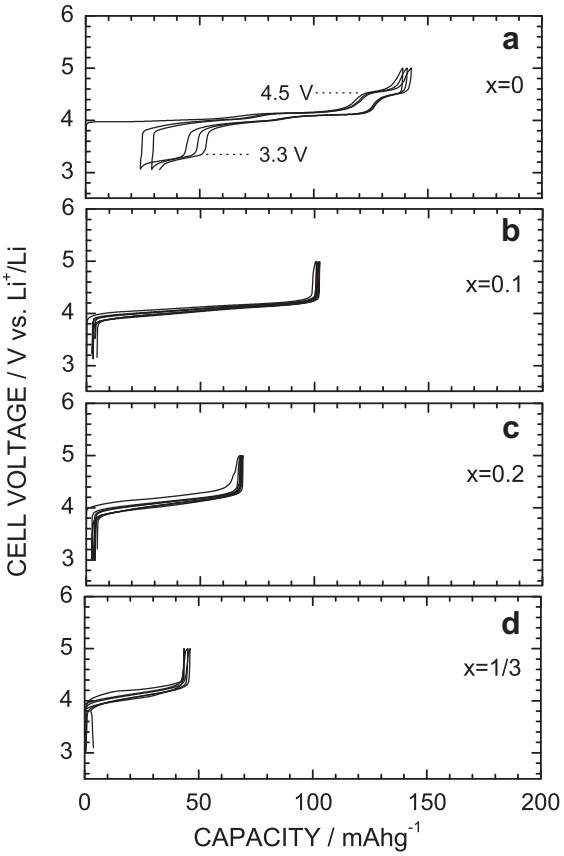

Fig. 3. Charge and discharge curves for the $Li/Li[Li_xMn_{2-x}]O_4$ cells with (a) $x = 0$, (b) $x = 0.1$, (c) $x = 0.2$, and (d) $x = 1/3$ operated at current density of 0.25 mA cm^{-2} at 298 K.

transition is around 280 K and that the structural phase transition is caused by the cooperative Jahn–Teller (JT) transition induced by Mn^{3+} ions with $t_{2g}^3e_g^1$ ($S = 2$). The crystal structure for the present $x = 0$ sample at 100 K is well explained by the single orthorhombic phase (*Fddd*), in which the unit cell is represented as $3a' (=a_o) \times 3b' (=b_o) \times c' (=c_o)$, where a', b', and c' are the lattice parameters of the pseudocubic spinel phase and a_o, b_o, and c_o are those of the orthorhombic superstructure phase [19]. For the samples with $x \geq 0.1$, the crystal structure at 100 K is essentially the same to those at $T > 100$ K; the cubic spinel phase ($Fd\bar{3}m$) for the samples with $x = 0.1$ and 0.2 and a mixture of cubic spinel phase ($Fd\bar{3}m$) and the Li_2MnO_3 phase ($C2/m$) for the $x = 1/3$ sample.

3.2. Electrochemical properties of $Li[Li_xMn_{2-x}]O_4$

Fig. 3 shows the charge and discharge curves for the Li/Li $[Li_xMn_{2-x}]O_4$ cells with (a) $x = 0$, (b) $x = 0.1$, (c) $x = 0.2$, and (d) $x = 1/3$. The cells were operated in the voltage range between 3.0 and 5.0 V at current density of 0.25 mA cm^{-2} at 298 K. For the $x = 0$ sample, the charge capacity is about 140 mAh g^{-1} at the first cycle, but decreases cycle by cycle. As described in 3.1 Section, the crystal structure for $x = 0$ keeps the cubic spinel phase ($Fd\bar{3}m$) at 300 K. Hence, the capacity fading for $x = 0$ is attributed to the formation and disappearance of the "double hexagonal phase" [25] which corresponds to the voltage plateau around 4.5 and 3.3 V, respectively. Other contribution would come from the dissolution of Mn ions from the lattice [30,31]. The excellent cycleability is obtained for the $x \geq 0.1$ samples, while the rechargeable capacity (Q_{recha}) decreases with increasing x. If the Q_{recha} value for LMO is determined by the amount of Mn^{3+} ions, more correctly, the electrochemical reaction of LMO proceeds as follow,

$$\mathrm{Li}\left[\mathrm{Li}_x\mathrm{Mn}^{3+}_{1-3x}\mathrm{Mn}^{4+}_{1+2x}\right]\mathrm{O}_4 \leftrightarrow y\mathrm{Li}^+ + ye^- + \mathrm{Li}_{1-y}\left[\mathrm{Li}_x\mathrm{Mn}^{3+}_{1-3x-y}\mathrm{Mn}^{4+}_{1+2x+y}\right]\mathrm{O}_4 \quad (y = 1-3x) \tag{2}$$

Q_{recha} at $x = 1/3$ should be 0 mAh g^{-1}, because all the Mn ions are in the 4 + state. The Q_{recha} value for the $x = 1/3$ sample is, however, about 45 mAh g^{-1}. This is caused by the presence of the Li_2MnO_3 impurity as illustrated in Figs. 1 and 2. The $W(Li_2MnO_3)$ value is almost consistent with the result of electrochemical charge and discharge tests, because the Q_{recha} value for the rest of spinel phase, i.e. $Li[Li_{0.21}Mn_{1.79}]O_4$ is calculated to be ~56 mAh g^{-1}. However, it should be noted that our recent muon-spin rotation/relaxation (μSR) study on the $x = 1/3$ compound reveals that the distribution of Li^+ ions at the 16*d* site is microscopically inhomogeneous [24]. Here, μSR is very sensitive to local magnetic environment and is an effective technique for investigating the (volume) fraction of each different phase in a sample.

3.3. Coefficients of thermal expansion for $Li[Li_xMn_{2-x}]O_4$

Fig. 4 shows the T dependence of cubic lattice parameter (a_c) and orthorhombic lattice parameters (a_o, b_o, and c_o) for the LMO samples with (a) $x = 0$ and (b) $x = 0.05$, 0.1, 0.15, 0.2, and 1/3. As T decreases from 400 K, a_c for the $x = 0$ sample decreases almost linearly down to 300 K, and then separates into the three orthorhombic lattice parameters of a_o, b_o, and c_o at 282.5 K ($=T_{JT}$) due to the cooperative JT transition. The present T_{JT} is almost comparable with the magnetic anomalies in the susceptibility (χ) at 290 K [32]

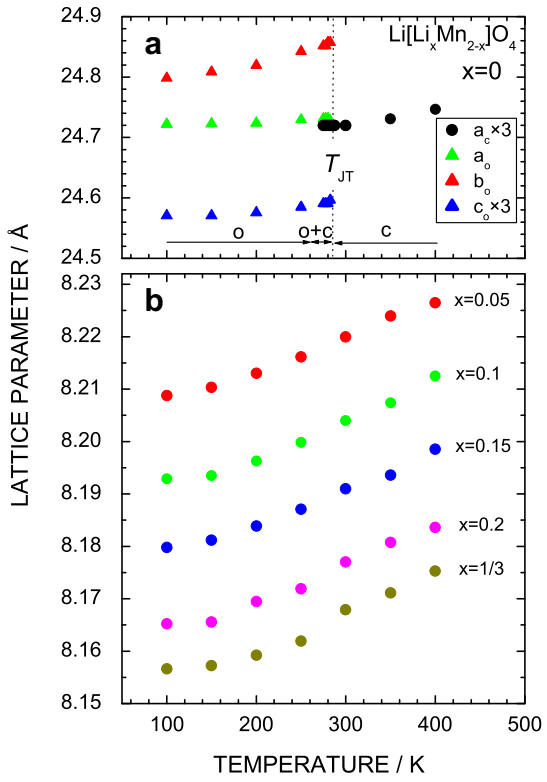

Fig. 4. Temperature (T) dependence of cubic lattice parameter (a_c) and orthorhombic lattice parameters (a_o, b_o, and c_o) for the Li[Li$_x$Mn$_{2-x}$]O$_4$ samples with (a) $x = 0$ and (b) $x = 0.05$, 0.1, 0.15, 0.2, and 1/3. T_{JT}, c, and o stand for the T of the cooperative Jahn–Teller (JT) transition, cubic, and orthorhombic, respectively. The lattice parameters of a_c and c_o for the $x = 0$ sample are multiplied by three for comparison.

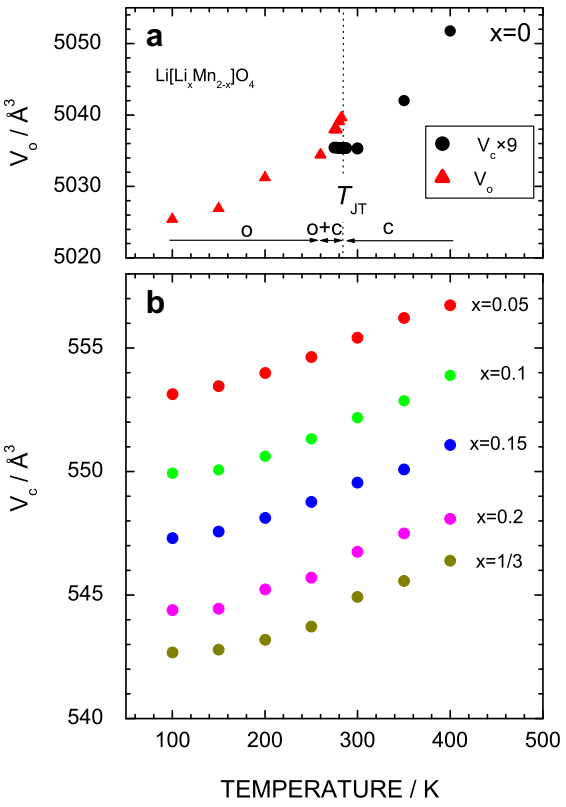

Fig. 5. Temperature (T) dependence of cubic lattice volume (V_c) and orthorhombic lattice volume (V_o) for the Li[Li$_x$Mn$_{2-x}$]O$_4$ samples with (a) $x = 0$ and (b) $x = 0.05$, 0.1, 0.15, 0.2, and 1/3. T_{JT}, c, and o stand for the T of the cooperative Jahn–Teller (JT) transition, cubic, and orthorhombic, respectively. The cubic lattice volume of V_c for the $x = 0$ sample is multiplied by nine for comparison.

and μSR measurements at 280 K [33]. Note that the cubic phase for the $x = 0$ sample is observed even below T_{JT}; a mixture of the cubic phase ($Fd\bar{3}m$) and the orthorhombic phase ($Fddd$) is stable in the T range between 282.5 and 270 K, whereas the single orthorhombic phase ($Fddd$) appears below 250 K. This is due to the phase transition of the first kind as probed by a differential scanning calorimetry (DSC) [17]. For the samples with $x \geq 0.05$, the a_c values decrease almost linearly down to ~200 K, then decrease with changing the slope (da_c/dT) with further decreasing T.

As shown in Fig. 5(a), the lattice volume for the $x = 0$ sample indicates discontinuous T dependence at T_{JT}. That is, as T decreases from 400 K, V_o for the $x = 0$ sample decreases almost linearly down to ~300 K, then slightly increases at 282.5 K, and finally decreases linearly with further lowering T. Since $V_c = 5035.3(1)$ Å^3 at 285 K and $V_o = 5039.6(1)$ Å^3 at 282.5 K, about 0.1% of volume expansion occurs at the JT transition. This means that the crystal lattice of $x = 0$ undergoes the abrupt volume change near the room T without changing the Li composition. Here, although the $x = 0$ sample is in the single cubic phase ($Fd\bar{3}m$) above 300 K, the V_c value is converted into the V_o value ($V_oV_c \times 9$) for comparison. For the samples with $x \geq 0.05$, the T dependence of V_c is similar to that of a_c (see Fig. 5(b)).

The average coefficient of linear thermal expansion (α_L) at 300 K is calculated as follow:

$$\alpha_L = \frac{\Delta l}{\Delta T \times l(300\ \mathrm{K})}, \tag{3}$$

where l is the length of lattice parameter such as a_c and a_o, and l(300 K) is the l at 300 K [l(285 K) is used only for the $x = 0$ sample]. As shown in Fig. 6(a), the α_L values for the $x = 0$ sample are quite different between the three orthorhombic axes, that is, $\alpha_L = 1.3(1) \times 10^{-6}$ K^{-1} along the a_o-axis, $\alpha_L = 13.1(1) \times 10^{-6}$ K^{-1} along the b_o-axis, and $\alpha_L = 5.7(1) \times 10^{-6}$ K^{-1} along the c_o-axis. In contrast to the linear decrease in a_c with increasing x, α_L for the samples with $x \geq 0.05$ ranges 7.2–8.0 $\times 10^{-6}$ K^{-1} (see Fig. 6(b)). Moreover, the α_L value which is calculated in the T range between 100 and 300 K shows similar x dependence.

For a cubic phase, the average coefficient of volumetric thermal expansion (β_V) can be calculated by $\beta_V = 3 \times \alpha_L$ assuming the isotropic expansion. Since the $x = 0$ sample is in the orthorhombic phase ($Fddd$) below 285 K, β_V is calculated as follow for comparison:

$$\beta_V = \frac{\Delta V}{\Delta T \times l(300\ \mathrm{K})}, \tag{4}$$

where V is the volume and V(300 K) is the V at 300 K. Fig. 6(b) shows the x dependence of β_V for the LMO samples. In contrast to anisotropic thermal expansion along the three orthorhombic axes, β_V for the $x = 0$ sample does not change between the T ranges; $\beta_V = 1.79(1) \times 10^{-5}$ K^{-1} at 100–285 K and $\beta_V = 1.74(1) \times 10^{-5}$ K^{-1} at 100–400 K. For the samples with $x \geq 0.05$, β_V is almost independent of x as in the case for α_L

4. Discussion

Table 1 summarizes the α_L and β_V values for the LMO samples. For the $x = 0$ sample, it is interesting to note that the α_L value of a_o-axis is quite small compared to that of c_o-axis, because a_o is longer than c_o. This can be understood by another phase transition below 100 K, that is, an antiferromagnetic (AF) transition with $T_N = 60$ K [18,20,33]. Fig. 7 shows the schematic illustration of the crystal

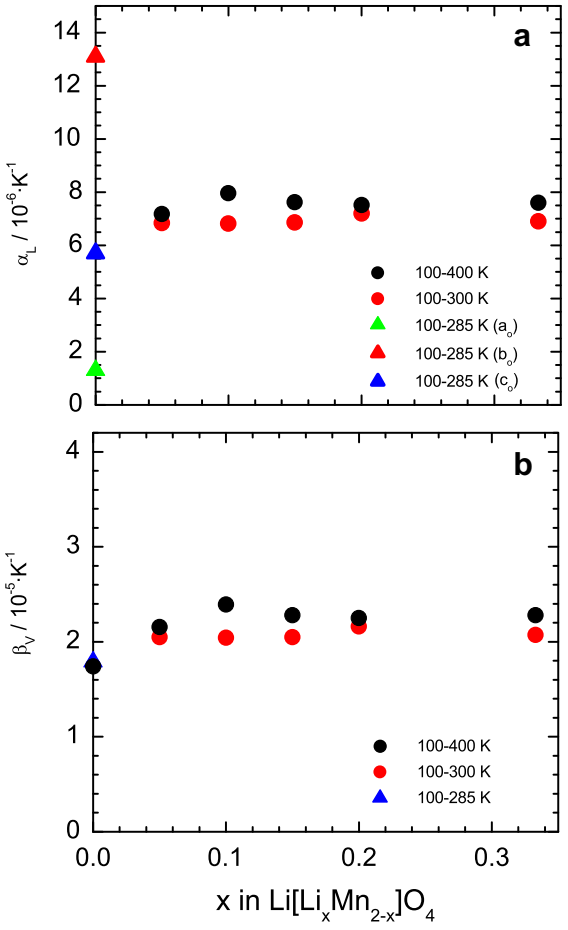

Fig. 6. Average coefficients of (a) linear thermal expansion (α_L) and (b) volumetric thermal expansion (β_V) for the $Li[Li_xMn_{2-x}]O_4$ samples with $0 \le x \le 1/3$.

structure of $x = 0$ in the orthorhombic phase (*Fddd*). Both Mn^{3+} spins with $S = 2$ ($t_{2g}^3 e_g^1$) and Mn^{4+} spins with $S = 3/2$ (t_{2g}^3) are coupled in the antiparallel mode (up and down) in the AF phase. Since the Mn^{3+}/Mn^{4+} arrangement of a_o-axis is same to that of b_o-axis, the small decrease in a_o with decreasing T stabilizes the charge ordering of Mn^{3+}/Mn^{4+} ions. In other words, the AF order is

Table 1
Average linear thermal expansion (α_L) and volumetric thermal expansion (β_V) for the $Li[Li_xMn_{2-x}]O_4$ samples with $0 \le x \le 1/3$ together with those for other lithium-ion battery materials.

Sample	$\alpha_L/10^{-6}$ K^{-1}	$\beta_V/10^{-5}$ K^{-1}	Range/K	Reference
$x = 0$[a]	1.3(1) (a_o) 13.1(1) (b_o) 5.7(1) (c_o)	1.74(1)	100–400	This work
$x = 0.05$	6.84(1)	2.16(1)	100–400	This work
$x = 0.1$	7.11(1)	2.39(1)	100–400	This work
$x = 0.15$	6.86(1)	2.28(1)	100–400	This work
$x = 0.2$	7.21(1)	2.25(1)	100–400	This work
$x = 1/3$[b]	6.94(1)	2.28(1)	100–400	This work
LiV_2O_4	7.29	2.18	5–300	[36]
$Fe[Li_{1/2}Fe_{3/2}]O_4$	3.15	0.94	10–300	[37]
$LiCoO_2$[c]	12.7 (a_h) 15.7 (c_h)	4.13(1)	90–300	[7]
$Li_{0.6}CoO_2$[c]	10.6 (a_h) 44.3 (c_h)	5.36(1)	90–300	[7]

[a] The α_L values are calculated in the temperature range between 100 and 285 K.
[b] The crystal structure is a mixture of the cubic spinel phase and the monoclinic Li_2MnO_3 phase.
[c] The lattice parameters are calculated in hexagonal setting.

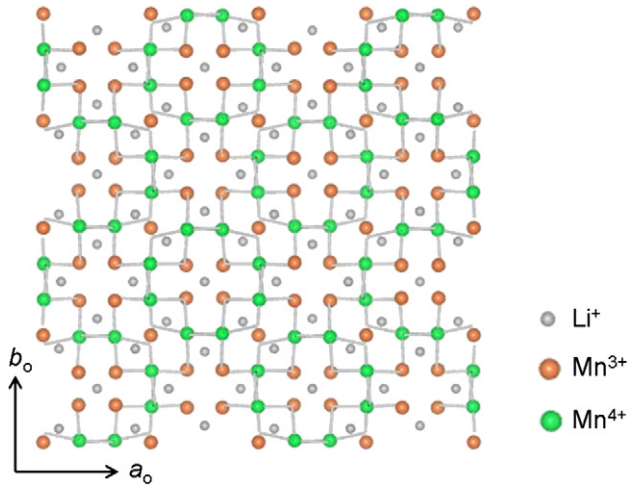

Fig. 7. Schematic illustration of the crystal structure of $LiMn_2O_4$ in the orthorhombic phase (*Fddd*). Although a_o is smaller than b_o down to 100 K, the Mn^{3+}/Mn^{4+} arrangement of a_o-axis is same to that of b_o-axis.

thought to be correlated with the anisotropic thermal expansion between the three orthorhombic lattice parameters.

The electrochemical measurements indicate that the partial substitution of Li ions at the 16*d* site improves the cycleability of charge and discharge reactions (see Fig. 3). This is consistent with the previous results on $Li[Li_xMn_{2-x}]O_4$ [28] and $Li[M_xMn_{2-x}]O_4$ (M = Cr, Co, and Ni) [34]. Although the authors in Refs. [28,34] explain that the improvement of their cycleability is caused by the strengthening of the bonds between the cation and O^{2-} ions, as x increases from 0, β_V slightly increases up to $x = 0.05$, and then keeps constant value ($\sim 2.2 \times 10^{-5}$ K^{-1}) with further increasing x (see Table 1). This suggests that the bond strength between the Mn(Li) and O^{2-} ions does not increase by the partial substitution for Mn ions. Since our μSR measurements demonstrate that the local JT distortion exists even for the $x = 0.15$ composition [33], the excellent cycleability for the samples with $x \ge 0.05$ is attributed to the inhibition of formation of double hexagonal phase around 4.5 V and/or dissolution of Mn ions.

The XRD density (d_{XRD}) at 300 K linearly decreases with increasing x, for example, $d_{XRD} = 4.293(1)$ g cm^{-3} for $x = 0$, $d_{XRD} = 4.236(1)$ g cm^{-3} for $x = 0.1$, and $d_{XRD} = 4.160(1)$ g cm^{-3} for $x = 0.2$. The x dependences of α_L and β_V show that the thermal expansion for LMO has no direct relation with d_{XRD}. This consideration is also supported by the facts that α_L for $MgAl_2O_4$ with $d_{XRD} = 3.58$ g cm^{-3} is almost the same ($\sim 9 \times 10^{-6}$ K^{-1}) to that for Co_3O_4 with $d_{XRD} = 6.05$ g cm^{-3} [35].

Comparing with other lithium battery materials, the α_L (or β_V) values for the LMO samples are almost similar to that for LiV_2O_4 [36] and about two times larger than that for $Fe[Li_{1/2}Fe_{3/2}]O_4$ [37]. Furthermore, the α_L values for $LiCoO_2$ and $Li_{0.6}CoO_2$ [7] are 2–6 times larger than those for LMO. From the view points of α_L and β_L, LMO is found to be suitable for the electrode materials for all solid-state LIB. If we assume that the operating T width of all solid-state LIB is 100 K centered at room T (-30 °C $\le T \le 70$ °C), the maximum volume change induced by the thermal difference is estimated as about 0.2% for all the LMO samples.

5. Conclusion

The coefficients of thermal expansion (CTE) in lithium manganese oxide spinels $Li[Li_xMn_{2-x}]O_4$ (LMO) were investigated by X-ray diffraction measurements. As x increases from 0, the average volumetric thermal expansion (β_V) slightly increases up to $x = 0.05$,

and then levels off at constant value ($\sim 2.2 \times 10^{-5}\,K^{-1}$) with further increasing x. This suggests that the bond strength between Mn(Li) and O^{2-} ions does not increase by the partial substitution of Li ions for Mn ions. The CTE values are effective to know the optimum conditions for all solid-state lithium-ion battery, because the solid–solid interface is usually constructed by heat treatment. Although we focused on the CTE for LMO in the present work, such studies on other lithium insertion materials together with their delithiated states are progress in our laboratory.

Acknowledgments

XRD experiment was performed at the SPring-8 with the approval of the Japan Synchrotron Radiation Research Institute (Proposal No. 2011A1854). We thank the staff of SPring-8 for help with the XRD measurements.

References

[1] G. Pistoia, Lithium Batteries, Elsevier, Amsterdam, 1993.
[2] J.W. Long, B. Dunn, D.R. Rolison, H.S. White, Chem. Rev. 104 (2004) 4463.
[3] L. Baggetto, R.A.H. Niessen, F. Roozeboom, P.H.L. Notten, Adv. Funct. Mater. 18 (2008) 1057.
[4] K. Mizushima, P.C. Jones, P.J. Wiseman, J.B. Goodenough, Mater. Res. Bull. 15 (1980) 783.
[5] J.N. Reimers, J.R. Dahn, J. Electrochem. Soc. 139 (1992) 2091.
[6] T. Ohzuku, A. Ueda, J. Electrochem. Soc. 141 (1994) 2972.
[7] K. Mukai, H. Nozaki, Y. Ikedo, J. Sugiyama, K. Ariyoshi, T. Ohzuku, J. Power Sources 192 (2009) 684.
[8] J.R. Dahn, U. von Sacken, M.W. Juzkow, H. Al-Janaby, J. Electrochem. Soc. 138 (1991) 2207.
[9] T. Ohzuku, A. Ueda, M. Nagayama, J. Electrochem. Soc. 140 (1993) 1862.
[10] T. Ohzuku, A. Ueda, N. Yamamoto, J. Electrochem. Soc. 142 (1995) 1431.
[11] C. Kittel, Introduction to Solid State Physics, third ed., Wiley, New York, 1968.
[12] R.S. Krishnan, R. Srinivasan, S. Devanarayanan, Thermal Expansion of Crystals, Pergamon, London, 1979.
[13] C. Zwikker, Physical Properties of Solids, Pergamon, London, 1954.
[14] J.C. Hunter, J. Solid State Chem. 39 (1981) 142.
[15] T. Ohzuku, M. Kitagawa, T. Hirai, J. Electrochem. Soc. 137 (1990) 769.
[16] T. Ohzuku, S. Kitano, M. Iwanaga, H. Matsuno, A. Ueda, J. Power Sources 68 (1997) 646.
[17] A. Yamada, M. Tanaka, Mater. Res. Bull. 30 (1995) 715.
[18] A.S. Wills, N.P. Raju, J.E. Greedan, Chem. Mater. 11 (1999) 1510.
[19] J. Rodriguez-Carvajal, G. Rousse, C. Masquelier, M. Hervieu, Phys. Rev. Lett. 81 (1998) 4660.
[20] I. Tomeno, Y. Kasuya, Y. Tsunoda, Phys. Rev. B 64 (2001) 094422.
[21] P. Piszora, J. Darul, W. Nowicki, E. Wolska, J. Alloy. Compd. 362 (2004) 231.
[22] J.M. Paulsen, J.R. Dahn, Chem. Mater. 11 (1999) 3065.
[23] S. Komaba, N. Yabuuchi, S. Ikemoto, J. Solid State Chem. 183 (2010) 234.
[24] K. Mukai, J. Sugiyama, Y. Ikedo, H. Nozaki, K. Kamazawa, D. Andreica, A. Amato, M. Månsson, J.H. Brewer, E.J. Ansaldo, K.H. Chow, J. Phys. Chem. C 114 (2010) 11320.
[25] M.R. Palacin, Y. Chabre, L. Dupont, M. Hervieu, P. Strobel, G. Rousse, C. Masquelier, M. Anne, G.G. Amatucci, J.M. Tarascon, J. Electrochem. Soc. 147 (2000) 845.
[26] E. Iwata, S. Takeda, M. Iwanaga, T. Ohzuku, Electrochemistry 71 (2003) 1187.
[27] M. Kitagawa, H. Wakabayashi, K. Ariyoshi, T. Ohzuku, ITE Lett. 8 (2007) 119.
[28] R.J. Gummow, A. de Kock, M.M. Thackeray, Solid State Ion. 69 (1994) 59.
[29] F. Izumi, T. Ikeda, Mater. Sci. Forum 198 (2000) 321.
[30] D.I. Jang, Y.J. Shin, S.M. Oh, J. Electrochem. Soc. 143 (1996) 2204.
[31] L.-F. Wang, C.-C. Ou, K.A. Striebel, J.-S. Chen, J. Electrochem. Soc. 150 (2003) A905.
[32] K. Mukai, J. Sugiyama, K. Kamazawa, Y. Ikedo, D. Andreica, A. Amato, J. Solid State Chem. 184 (2011) 1096.
[33] J. Sugiyama, K. Mukai, Y. Ikedo, P.L. Russo, T. Suzuki, I. Watanabe, J.H. Brewer, E.J. Ansaldo, K.H. Chow, K. Ariyoshi, T. Ohzuku, Phys. Rev. B 75 (2007) 174424.
[34] M. Kaneko, S. Matsuno, T. Miki, M. Nakayama, H. Ikuta, Y. Uchimoto, M. Wakihara, K. Kawamura, J. Phys. Chem. B 107 (2003) 1727.
[35] A. Petric, H. Ling, J. Am. Ceram. Soc. 90 (2007) 1515.
[36] D.C. Johnston, C.A. Swenson, S. Kondo, Phys. Rev. B 59 (1999) 2627.
[37] J. Darul, W. Nowicki, P. Piszora, E. Wolska, J. Alloy. Compd. 401 (2005) 60.